Title

Role of land surface processes in South American monsoon development

Permalink

Journal

ISSN

Authors

Xue, Y
de Sales, F
Li, W P
et al.

Publication Date

Peer reviewed

Role of Land Surface Processes in South American Monsoon Development

YONGKANG XUE

Department of Geography, and Department of Atmospheric Sciences, University of California, Los Angeles, Los Angeles, California

F. DE SALES AND W.-P. LI*

Department of Geography, University of California, Los Angeles, Los Angeles, California

C. R. MECHOSO

Department of Atmospheric Sciences, University of California, Los Angeles, Los Angeles, California

C. A. NOBRE

Centro de Previsão de Tempo e Estudos Climáticos/INPE/MCT, Cachoeira Paulista, Brazil

H.-M. JUANG

NOAA/NCEP, Camp Springs, Maryland

(Manuscript received 25 January 2005, in final form 28 July 2005)

ABSTRACT

This study explores the role of vegetation biophysical processes (VBPs) in the structure and evolution of the South American monsoon system (SAMS) with an emphasis on the precipitation field. The approach is based on comparing ensemble simulations by the National Centers for Environmental Prediction general circulation model (GCM) in which the land surface parameterization in one ensemble includes an explicit representation of vegetation processes in the calculation of surface fluxes while the other does not [GCM/ Simplified Simple Biosphere Model (SSiB) and GCM/Soil, respectively], but with similar monthly mean surface albedo and initial soil moisture. The ensembles consist of five pairs of 1-yr integrations differing in the initial conditions for the atmosphere. The results show that, during the austral summer, consideration of explicit vegetation processes does not alter the monthly mean precipitation at the planetary scale. However, at continental scales, GCM/SSiB produces a more successful simulation of SAMS than GCM/Soil. The improvement is particularly clear in reference to the seasonal southward displacement of precipitation during the onset of the SAMS and its northward merging with the intertropical convergence zone during the monsoon mature stage, as well as better monthly mean austral summer precipitation over the South American continent.

The changes in surface water and energy balances and circulation in October (monsoon onset) and December (the start of the monsoon mature stage) were analyzed for a better understanding of the results and mechanisms involved. It was found that the major difference between the simulations is in the partitioning of latent heat and sensible heat fluxes (i.e., different Bowen ratio), which produced different latitudinal and longitudinal thermal gradients at the surface. A stronger sensible heat flux gradient between continent and ocean in the GCM/SSiB simulation helped generate an enhanced ventilation effect, which lowered moist static energy (MSE) over the northeast coast of South America leading to stronger counterclockwise turning of the low-level wind from the Atlantic Ocean toward the continent during the premonsoon and early monsoon stages, modifying moisture flux convergence (MFC). It was further iden-

* Current affiliation: National Climate Center, Beijing, China.

Corresponding author address: Dr. Yongkang Xue, Department of Geography, University of California, Los Angeles, Los Angeles, CA 90095.
E-mail: yxue@geog.ucla.edu

tified that the seasonality of savanna and shrublands to the south and east of the Amazon rain forest contributed to the variability of heating gradients and influenced the SAMS onset and its northward merge with the ITCZ at the early monsoon mature stage. The comparison of the differences between precipitation, evaporation, advection of MSE, and MFC based on simulations using two different land parameterizations suggested that the VBP modulated the surface water budget, but its impact on precipitation was determined by the changes in circulation via changes in heat gradient and MSE.

1. Introduction

It has been recognized in the last decade that the South American monsoon system (SAMS), which dominates the warm-season circulation over South America, is the second largest monsoon system in the world (Zhou and Lau 1998; Marengo et al. 2001; Nogués-Paegle et al. 2002). The SAMS is characterized by intense precipitation over central Brazil and Bolivia in a region that is linked to the Atlantic intertropical convergence zone (ITCZ) to the northeast and extends into the South Atlantic convergence zone (SACZ) to the southeast. The most important characteristics of the circulation include the Bolivian high, a high air pressure system centered over the Bolivian plateau at upper atmospheric levels, and a surface low over northern Argentina, known as the Chaco low. The trade winds from the tropical Atlantic Ocean provide the major moisture source for the SAMS. A strong low-level jet [referred to as the South American low-level jet (SALLJ)] along the eastern slopes of the Andes is a key contributor to the moisture flux from the Tropics to the midlatitudes with the strongest winds over Bolivia (Nogués-Paegle and Mo 1997; Berbery and Barros 2002). The SALLJ is active during the entire year. The SACZ extends cloudiness and precipitation southeastward from the southern Amazon toward southeast Brazil and the neighboring Atlantic Ocean and is present in the southern spring and summer (October through March). Its variability extends the effects of monsoon variability farther south into Argentina and Uruguay.

In the SAMS, as in all monsoons, ocean–continent contrasts are of fundamental importance. In addition, several studies have indicated that remote variability of the ocean–atmosphere system in the Pacific and Atlantic Oceans can contribute to the variability of SAMS on several time scales. The extreme phases of the El Niño–Southern Oscillation (ENSO) cycle have a significant impact on the overall strength of the SAMS and the spatial distribution of precipitation over tropical South America (e.g., Kousky et al. 1984; Ropelewski and Halpert 1987; Fu et al. 2001; Nogués-Paegle et al. 2002; Lau and Zhou 2003). In general, sea surface temperature (SST) anomalies in the eastern equatorial Pacific and rainfall in the core region of the SAMS tend to be anticorrelated, as rising air in the former region is as-

sociated with sinking air in the latter one. ENSO also significantly influences southern Brazil, eastern Argentina, and Uruguay (Pisciottano et al. 1994; Grimm 2000). Pisciottano et al. showed that in southeastern South America rainfall tends to be higher than average in warm ENSO years, especially in November–January, and lower than average in years with a cold ENSO phase, especially in October–December. Mechoso and Perez-Iribarren (1992) demonstrated that this effect is also apparent in river runoff.

The interannual variability of SSTs over the tropical Atlantic has a strong influence on the distribution of rainfall over the tropical Americas (Moura and Shukla 1981; Hastenrath and Heller 1977). Over the southwest Atlantic, interannual intensifications of the SACZ have also been linked to SST anomalies (Nogués-Paegle et al. 2002). Furthermore, the decadal rainfall variation presents a pattern of meridional shift of the ITCZ on both the eastern Pacific and western Atlantic Ocean, which is closely related to the decadal change of the cross-equatorial SST gradient (Nobre and Shukla 1996; Rao et al. 1999).

The Amazon Basin of South America is the largest continuous region of tropical forest in the world. Here, deforestation has been intense during the past three decades. The possible impact of Amazon deforestation on the South American regional climate has been a major scientific and social issue for more than a decade (e.g., Dickinson and Henderson-Sellers 1988; Nobre et al. 1991; Eltahir and Bras 1993; Xue et al. 1996a; Zeng et al. 1996; Henderson-Sellers and Pitman 2002; Weaver and Avissar 2001; Tanajura et al. 2004, manuscript submitted to *Earth Interactions*). Most studies performed so far with general circulation and regional climate models (GCM and RCM, respectively) suggest that large-scale deforestation would result in a local reduction in precipitation. In most of these modeling studies, land surface conditions are drastically changed at large scales. To our knowledge, no analysis has discussed desertification impacts in the framework of the SAMS. SAMS should provide a useful framework for understanding South American circulation and the impact of deforestation during the warm season.

Differential heating of the land and ocean and latent heat release into the atmosphere contribute to deter-

mine the evolution, strength, and spatial distribution of large-scale monsoons (Webster et al. 1998). It is important, therefore, to investigate the role that land surface processes can play in modulating the monsoon circulation and surface hydrology. In a GCM sensitivity study, Sato et al. (1989) used two different parameterizations of land surface processes: 1) the bucket model (Budyko 1974), which models land as a bucket with a 150-mm rainfall equivalent capacity, and 2) the Simple Biosphere Model (SiB: Sellers et al. 1986), which treats the vegetation explicitly by incorporating the vegetation biophysical processes (VBPs) with the exchanges of energy and water between land and atmosphere. Sato et al.'s study demonstrated that explicit inclusion of VBP produced substantially different and more realistic summer seasonal mean precipitation over continents as well as over oceans (Sato et al. 1989). However, an outstanding issue is whether this improvement is due to the explicit VBP treatment or just to the different monthly mean vegetation albedo and surface roughness length, whose importance in climate simulation has been demonstrated by a number of studies (e.g., Charney et al. 1977; Sud et al. 1988). In other words, the role and mechanisms of VBP effects, excluding monthly mean albedo and surface roughness length, in land–atmosphere interactions remains unclear. This is an important issue because it is relevant to many parameterizations, such as radiative transfer in the canopy, evapotranspiration from three components (soil evaporation, water interception loss, and photosynthesis-controlled canopy transpiration), and modified aerodynamic resistance by vegetation, as well as a large amount of data collection, such as seasonal varied surface vegetation properties, including leaf area index (LAI), etc.

Xue et al. (2004) have compared ensemble simulations of the East Asian–African monsoon by the National Centers for Environmental Prediction (NCEP) GCM in which the land surface parameterization in one ensemble includes an explicit representation of vegetation processes (Xue et al. 1991) in the calculation of surface fluxes while the other does not [GCM/ Simplified Simple Biosphere Model (SSiB) and GCM/ Soil, respectively]. Each ensemble consists of simulations for a 5-month period corresponding to the northern warm season of 1987 that differ in the initial conditions for the atmosphere but have the same initial conditions in soil moisture and similar monthly mean surface albedo and roughness length. The two ensembles produced similar results at the planetary scale but substantially different results in the monsoon regions and some continental areas. In GCM/Soil, the moisture transport and precipitation were too strong in the premonsoon season, and the abrupt northward

jump and large-scale turning of the low-level circulation during the early monsoon stage (Xue 2005) that characterize the East Asian summer monsoon were either unclear or not simulated. GCM/SsiB, on the other hand, was able to capture these two important features in the monsoon evolution. An analysis of the simulations showed that the two land surface representations produced different longitudinal and latitudinal gradients of sensible surface heat and pressure gradients, as well as low-level temperature, that affected wind flow (through geostrophic balance), and moisture transport. These results suggest that the strong east–west thermal gradient may contribute to the abrupt northward jump of the East Asian monsoon, and the latitudinal heating gradient may contribute to the clockwise and counterclockwise turning of the low-level wind on the east Asian and African continents.

Land surface–atmosphere interactions are complex and depend on many factors. The land effects do not always dictate that more vegetation causes more evaporation and then more precipitation. The monsoon is a complex system. Some areas would be dry where the monsoon either was delayed or could not reach any farther, and others would be wet due to redistribution of the circulation or changes in position of the maximum precipitation band. More comprehensive research on the effects of land surface processes on different monsoon systems is necessary.

In this study we followed the same approach as in our East Asian/African monsoon study (Xue et al. 2004). Thus, we used the NCEP GCM (Kalnay et al. 1990; Kanamitsu et al. 2002) coupled to the SSiB (Xue et al. 1991, 1996b) and compared results with those from the same GCM coupled with a land scheme in which the biophysical processes were not explicitly parameterized. Using these comparisons, Xue et al. (2004) explored the influence of the VBP in a soil/vegetation complex on intraseasonal monsoon development. Here, we focused on the impact of VBP on the SAMS.

2. Model descriptions

The GCM that we used was a recent version of the NCEP seasonal forecast model (Kanamitsu et al. 2002) placed on the Concurrent Versions System (CVS) server. The NCEP GCM includes the Moorthi and Suarez (1992) convection scheme, the Chou (1992) and Chou and Suarez (1994) radiation scheme, and the Hong and Pan (1996) nonlocal planetary boundary layer scheme. The computer code of this version was extensively modified to make it compatible with multiple platforms that use single and/or multiple shared memories. All changes were incorporated using a pre-

processor technique such that the same original code works on single and multiple processors as well as on massively parallel processor platforms. The model, after implementing the SSiB, was extensively tested to ensure that the result from single node and different multiple processes are bit-by-bit equivalent. We used the model version with 18 levels and T42 horizontal resolution.

To test the impact of VBP at the land surface on the SAMS, two land surface parameterizations were used in the GCM as in the study of Xue et al. (2004). One was a simple two-layer soil model and the other was a biophysical model, SSiB. The two land parameterization schemes represent different land surface processes. In NCEP GCM/Soil, which was used in the original NCEP GCM, the ground hydrology was simulated by the soil model. No explicit biophysical processes were included. The distributions of monthly mean vegetation albedo and surface roughness length were prescribed based on the Dorman and Sellers (1989) dataset, which had monthly mean values similar to those used in SSiB. Soil temperature and soil volumetric water content were computed in two layers at depths 0.1 and 1.0 m with an implicit time integration scheme (Pan and Mahrt 1987). The lowest atmospheric model layer was the surface layer, where the Monin–Obukhov similarity profile relationship was applied to obtain the surface stress and sensible and latent heat fluxes (Miyakoda and Sirutis 1986). A bulk aerodynamic formula was used to calculate the fluxes once the turbulent exchange coefficients had been obtained.

In SSiB, the soil moisture was calculated with an approach similar to NCEP's two-layer soil model, but many vegetation–atmosphere interaction processes were included. For example, the radiative transfer in the canopy was simulated, which produced a diurnal variation in surface albedo. SSiB included processes such as water interception loss, direct evaporation from bare soil, and canopy transpiration (controlled by photosynthesis) to describe the surface water balance. Similarity theory was used to calculate the aerodynamic resistance from the canopy to the reference height. Based upon the Paulson (1970) and Businger et al. (1971) equations, a relationship between the Richardson number, vegetation properties, and aerodynamic resistance at the vegetated surface was developed (Xue et al. 1991, 1996b). In SSiB, the resistance of the neutral part was dependent on vegetation and soil properties. In the nonneutral part, a parameterization was related to atmospheric stability conditions. In addition, some adjustments based on the vegetation conditions were introduced. A global land cover map based on remote sensing (Hansen et al. 2000) was used in NCEP GCM/
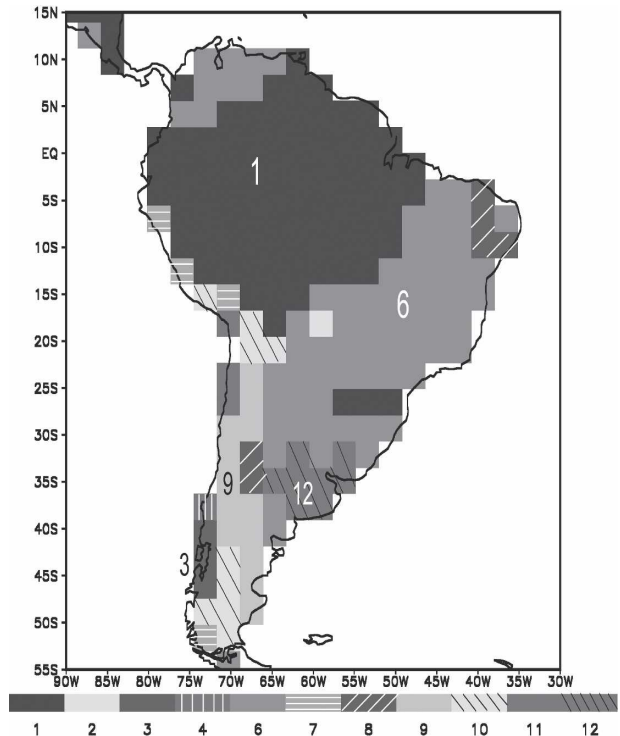

FIG. 1. The NCEP GCM/SSiB Land Cover Classification Map for South America. Type 1: tropical rain forest; type 2: broadleaf deciduous trees; type 3: broadleaf and needleleaf trees; type 4: needleleaf evergreen trees; type 5: needleleaf deciduous trees; type 6: broadleaf trees with ground cover; type 7: grassland; type 8: broadleaf shrubs with ground cover; type 9: broadleaf shrubs with bare soil; type 10: dwarf trees with ground cover; type 11: desert; type 12: crops; and type 13: permanent ice.

SSiB, with some improvement over South America based on the data from the Centro de Previsão de Tempo e Estudos Climáticos (CPTEC). Figure 1 shows the vegetation classification map for the South American region. The reader is referred to Xue et al. (2004) for more detailed information on this map and vegetation parameters used in the coupled GCM/SSiB model.

3. Experimental design and initial and boundary conditions

The NCEP–National Center for Atmospheric Research (NCAR) global reanalysis fields (Kalnay et al. 1996; Kistler et al. 2001) provided the initial conditions in both case C and case S1 for the atmosphere, soil moisture, and soil temperatures; ocean surface boundary conditions (SST and sea ice); and initial snow depth, as used by NCEP for prediction/forecasting. We selected 30 April and 1, 3, 4, and 5 May 1987 as the starting dates for model simulations; 2 May 1987 was skipped due to errors detected in the data for that day:

1987 was an ENSO year and was one of two years for which a comprehensive soil moisture dataset (Dirmeyer et al. 1999) was available at the time of our experiments. Soil moisture was simulated without nudging in all cases. Specified SST and sea ice were updated using observational data during the simulation. The GCM/Soil and GCM/SSiB ensemble simulations are referred to in this paper as cases C and S1, respectively. Comparisons between the results obtained in the two ensembles would mainly indicate the effects of explicit description of VBP in the GCM.

The impact of initial soil moisture on the model simulations was studied using soil moisture data from the Global Energy and Water Cycle Experiment (GEWEX) soil wetness project (GSWP) (Dirmeyer et al. 1999). One additional set of 1-yr simulations with GCM/SSiB (referred to as case S2) was conducted using the GSWP soil moisture as initial soil moisture for the same five atmospheric initial dates as case S1. The comparisons between cases S1 and S2 indicate the effects of different initial soil moisture.

4. Simulation results

a. General features

Figure 2a is the December–February (DJF) mean precipitation from the Climate Prediction Center Merged Analysis of Precipitation (CMAP) (Xie and Arkin 1997) in which observations from rain gauges are merged with estimates from several satellite-based algorithms (infrared and microwave). Case C simulated DJF precipitation reasonably well (Fig. 2b). The ITCZs over the Pacific and Atlantic were well defined north of the equator. A strong South Pacific convergence zone (SPCZ) was captured. The observed Australian monsoon was weak, and monsoon rain over the Australian continent fell mainly in December in 1987 (not shown). Case C failed to simulate the monsoon rain in December (not shown) and only obtained a weak value of DJF precipitation to the north of Australia (Fig. 2b). The monsoon precipitation in South America was simulated, including the SACZ, albeit its location was too far north and the western Amazon along the Andes was dry. These deficiencies have been found in a number of austral summer season simulations for South America (Cavalcanti et al. 2002). In addition, case C simulated too much precipitation in the eastern Pacific near Central America and the ITCZ over the Atlantic, as well as an excessively large area of light precipitation at higher southern latitudes (Fig. 2b).

As in the Northern Hemisphere summer (Xue et al. 2004), cases S1 and C produced very similar spatial distributions of precipitation at the planetary scale (Fig.
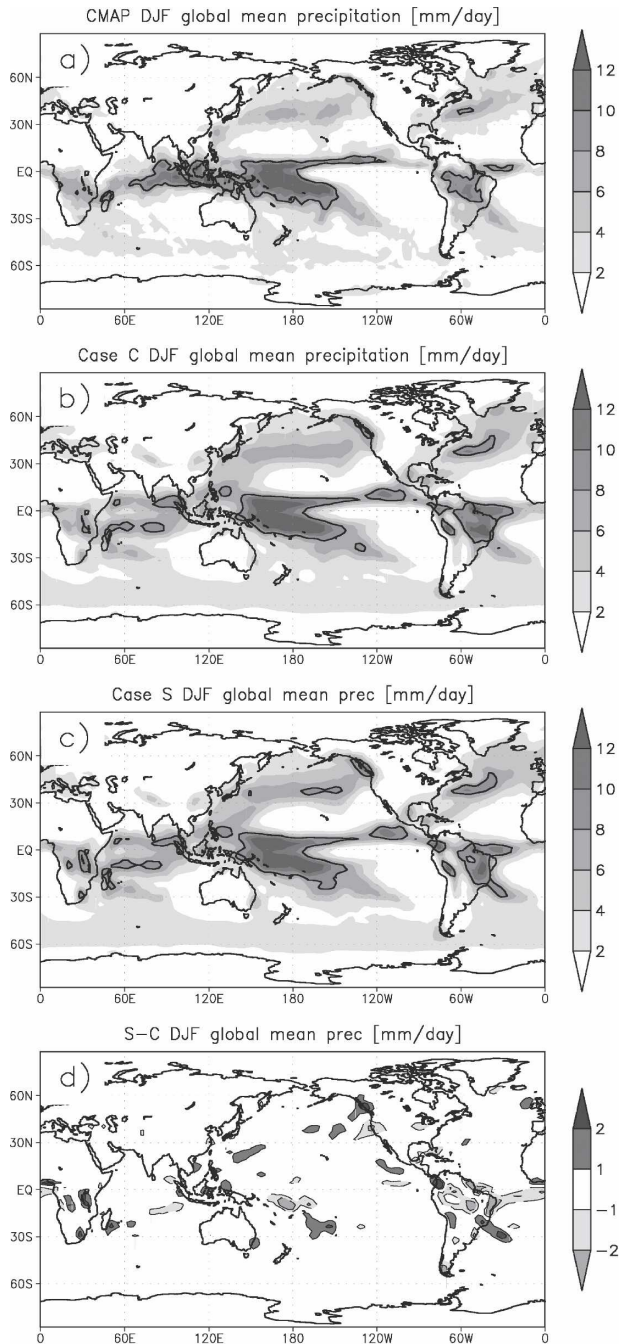

FIG. 2. DJF 1987/88 precipitation for (a) CMAP, (b) case C, (c) case S1, and (d) case S1 − case C (mm day^{-1}). The bold lines in (a)–(c) are 8 mm day^{-1} contour lines.

2c). There were, however, substantial differences in the SAMS region (Fig. 2d) with significance at the 90% level in the Student's t test (not shown). Similar to Sato et al. (1989), the changes of land surface parameterizations also affected the precipitation over ocean due to the impact of land–atmosphere interaction on circula-

	Precipitation				Evaporation	
	Observation	Case C	Case S1	Case S2	Case C	Case S1
Annual	114	137	123	121	111	83
Jan	144	180	162	163	128	95
Feb	158	187	180	175	128	97
Mar	141	178	170	162	121	93
Apr	149	151	146	140	108	84
May	111	128	109	110	107	80
Jun	92	98	90	86	91	75
Jul	91	84	81	80	90	73
Aug	64	76	73	71	91	71
Sep	75	97	80	77	102	74
Oct	102	136	107	116	116	81
Nov	119	150	127	126	124	90
Dec	128	175	149	149	130	93

tion, albeit with much reduced magnitude and scope. Compared to case C, case S1 shifted the SACZ back to the south and reduced precipitation in the eastern Amazon and Atlantic ITCZ. Table 1 shows the annual and monthly mean precipitation over the South American continent. Case S1 persistently and substantially improved the simulations of monthly mean precipitation except for April and July, two dry months for South America, in which both cases had similar results. The most substantial improvement corresponded to October through January, which were the crucial months for development of the SAMS.

This simulation and the results from our previous study (Xue et al. 2004) suggest that the VBP, excluding surface monthly mean albedo and initial soil moisture, mainly have influence on wet season precipitation over the continental convective regions, which are located within the monsoon regions. In the next sections, we further examine whether/how these regional differences were associated with VBP.

b. Evolution of the SAMS

Figure 3 illustrates the monsoon evolution in the form of precipitation maps corresponding to the second 10-day period of the selected month. In 1987 during the late austral winter, precipitation was intense around the equator with local maxima over the Caribbean coast of Venezuela, Colombia, and Guyana, while Amazonia was very dry (Fig. 3a). Both cases C and S1 simulated these features (Figs. 3b and 3c). The simulated precipitation maximum, however, was higher over land, and the ITCZ was weaker over the eastern Pacific compared with CMAP. The precipitation over the midlati-

tude southern Atlantic Ocean was also simulated by both models but with a lower maximum along the southeast South American coast compared with observations. Up to this point, therefore, the two simulations produced similar results (also indicated in Table 1). Nevertheless, case C produced excessive precipitation along the Andes and weak precipitation along the southwest coast of South America.

The subsequent development phase of SAMS during austral spring of 1987 was characterized by a rapid southeastward shift of the region of intense convection from the equator toward the southern Amazon Basin and the Brazilian highlands, which was completed within a 1-month time period. The second 10-day mean for October shows a maximum precipitation (4–6 mm day^{-1}) in the central Amazon. The SACZ extended over the southern Atlantic Ocean along the midlatitude southeast coast (Fig. 3d). Both case C and case S1 simulated the southeastern spreading of precipitation and a dry northeastern Brazil in October (Figs. 3e and 3f). The extension of precipitation into the Andes and the SACZ over southeast Brazil and the nearby Atlantic, however, was stronger than that in CMAP (Fig. 3d). The heavy precipitation (4–8 mm day^{-1}) in case S1 moved to the central Amazon (Fig. 3f), consistent with observations. Case C, on other hand, produced a much faster propagation of precipitation (Fig. 3e) than CMAP and case S1, with a more homogeneous northwest–southeast precipitation band that extended from 5°N to 25°S. The precipitation values were very high compared to the observation (6–12 mm day^{-1}).

The location of the maximum precipitation extended toward the southeast in November and December (Fig. 3g). Both cases C and S1 showed the extension of rainfall into southeastern South America in December and heavy rainfall in the central Amazon and southeastern Brazil. In addition, an active SACZ was also simulated (Figs. 3h and 3i). The precipitation in case C was much heavier, with more than 10 mm day^{-1} over the monsoon region (see section 4.3 and Fig. 9 for more detailed discussion.). In addition, case C also produced a strong rainfall branch along the northeast South American coast, which merged the monsoon precipitation with the ITCZ. In observations, there is a clear separation between the region of monsoon rain over the continent and the ITCZ over the Atlantic Ocean, and northeastern Brazil was rather dry in December 1987 (Fig. 3g). Different from case C (Fig. 3h), a weaker northeast extension was produced in case S1 (Fig. 3i). The intensity of the precipitation was also much closer to observations (Table 1).

The mature and decay phases of SAMS continue through austral summer as convection gradually re-
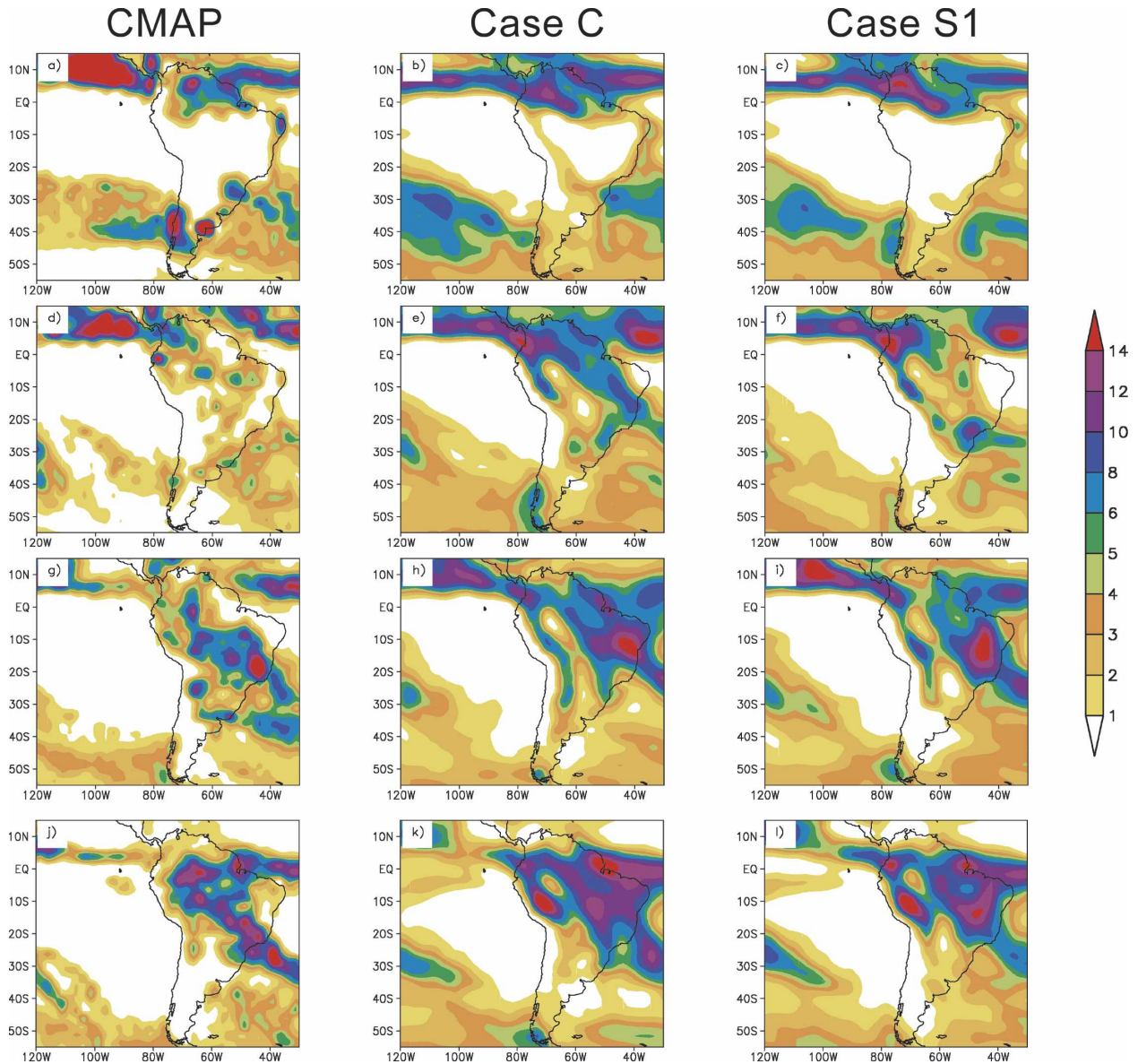
FIG. 3. Ten-day mean precipitation (mm day^{-1}) for the second 10 days of following month: (a) August 1987 (CMAP), (b) August 1987 (case C), (c) August 1987 (case S1), (d) October 1987 (CMAP), (e) October 1987 (case C), (f) October 1987 (case S1), (g) December 1987 (CMAP), (h) December 1987 (case C), (i) December 1987 (case S1), (j) February 1988 (CMAP), (k) February 1988 (case C), and (l) February 1988 (case S1).

treats northward toward the equator merging with the ITCZ. In February, a strong precipitation band appeared along the equator (Fig. 3j). Both cases S1 and C simulated these features (Figs. 3k and 3l). The intensity, however, was stronger in case C over the monsoon region, and excessive light precipitation was present over southern South America after the monsoon withdrawal, as indicated in Table 1. The two cases also had heavy rain along the western slopes of the Andes. This feature was not present in CMAP. This deficiency was

probably due to difficulties in dealing with the topography at the model's coarse resolution.

To delineate more clearly the entire development process of the SAMS premonsoon and monsoon evolution during the rainy season, we illustrate in Fig. 4 the zonally averaged, 10-day mean precipitation between 60° and 40°W from September through April. Intense precipitation moved into the domain between 5° and 10°S in October with a tendency toward moving southeastward (Fig. 4a, dashed red arrow). The heavy rain
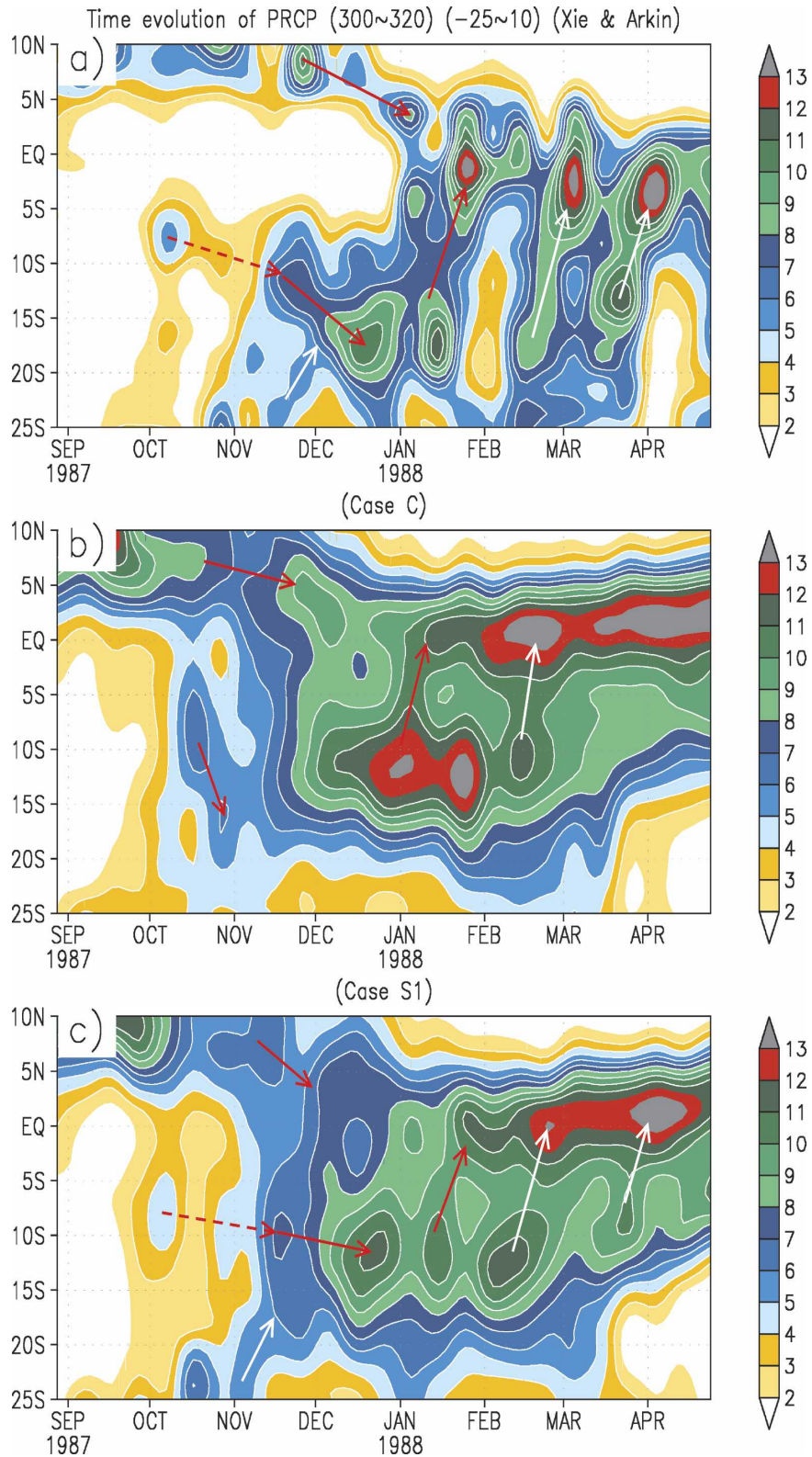
FIG. 4. Temporal evolution of the 10-day mean precipitation (mm day^{-1}) averaged over 40°–60°W from September through April: (a) CMAP, (b) case C, and (c) case S1.

(more than 6 mm day^{-1}) abruptly appeared between 10° and 15°S in November again after a relatively dry period and moved farther southward (solid red arrow). Meanwhile, a rainfall band moved northward from 25° to 15°S (solid white arrow). Northeastern South America was still very dry during October/December. The monsoon rain reached its southernmost position in December and then returned to the equator in January (solid red arrow) where it merged with the ITCZ (solid red arrow). These features are consistent with the SAMS evolution process described in a 1989–90 case study based on reanalysis and satellite data (Zhou and Lau 1998) and the 1979–2000 climatology based on CMAP (not shown).

There were clear differences between cases C and S1 in simulations of the monsoon evolution (Figs. 4b and 4c). Case C correctly simulated the rainy season and the heavy rainfall bands between the equator and 5°S and between 10° and 15°S (Fig. 4b). The precipitation in October, however, rapidly extended to around 18°S (red solid arrow) without a dry period, as pointed out earlier (Fig. 3e), and the southward development of precipitation in November and December was not simulated, inconsistent with CMAP (Fig. 4a). The dry band between 5°S and 5°N during November and December was replaced by a very wet period due to strong merging with the ITCZ as discussed earlier (Fig. 3h). Furthermore, the simulated rain in the wet season was more intense than that indicated by the observations (Fig. 4b and Table 1).

Case S1, on the other hand, simulated a southward development of precipitation from between 5° and 10°S to between 10° and 15°S (but still not south enough) compared to the observation during October–December with an abrupt rainy season starting in November (Fig. 4c, red dashed and solid arrows) and a northward rainfall band development between 25° and 15°S during November (Fig. 4c, white solid arrow). The merging of the monsoon with the ITCZ was still more intense than observed but was more realistic than in case C. The intensity during the wet season was close to observations (Table 1). By and large, the monsoon development processes were better simulated in case S1 than in case C. We will further discuss the implication of these differences and their causes in the next section.

There were additional monsoon northward propagations in February and March (Fig. 4a, white solid arrows) in CMAP. It is interesting to note that two cases produced different higher-frequency synoptic events during this time period (Figs. 4b,c, white solid arrows). We do not know, at this point in time, whether these differences were caused by VBP or by model internal variability. More case studies are required. In 1988,

there was also a distinguishable dry period between 20° and 5°S in January due to a blocking pattern over the subtropical Eastern Pacific, which brought dry, stable conditions that inhibited convection for weeks. This dry event was not well simulated by either model.

c. Physical and dynamic mechanisms of land surface and atmospheric effects

The differences between cases C and S1 were caused by the different parameterizations in land surface processes: one with explicit parameterizations of energy and water transfer in vegetation and soil processes and another only parameterizing soil processes. The two cases, however, had the same initial soil moisture and similar monthly mean surface albedo, which differentiates this work from a typical investigation of land cover change. Figure 5 shows the zonally averaged (60° to 40°W) differences in surface energy components between case C and case S1. There was no substantial difference in the sum of downward shortwave and long-wave radiation, nor upward shortwave radiation (not shown), due to similar monthly mean surface albedo. The upward longwave radiation had some differences owing to the relatively high surface temperature in case S1 (Fig. 5a). The most substantial differences found were in the partitioning between latent and sensible heat fluxes. For example, case S1 constantly produced lower latent heat flux and higher sensible heat flux (Figs. 5b and 5c). Furthermore, these differences exhibited high temporal and spatial variability with maximum changes in sensible and latent heat fluxes occurring during October–January. The lower evaporation in the SAMS in case S1 than in case C was consistent with the lower precipitation shown in Figs. 4b and 4c. The question is whether the differences in surface energy partitioning caused changes in monsoon precipitation or were merely a response to the changes in precipitation. To gain insight into the mechanisms at work, we next focus on October (monsoon onset) and December (the start of the monsoon mature stage), which were crucial months for the monsoon development and during which the sensible heat flux showed the largest differences between the two cases (Fig. 5c).

To achieve a better understanding of the mechanisms involved, we closely examined the differences of precipitation, evaporation, and sensible heat flux between CMAP, case C, and case S1 (Fig. 6). In October, case C produced a large positive bias in precipitation in the northeast Amazon and southeast Brazil (Fig. 6a) in its monsoon evolution processes discussed earlier (Figs. 3e, 4b). Meanwhile, the Atlantic extension of the SACZ shifted to the north and produced a dipole anomaly pattern (positive bias to the north and nega-
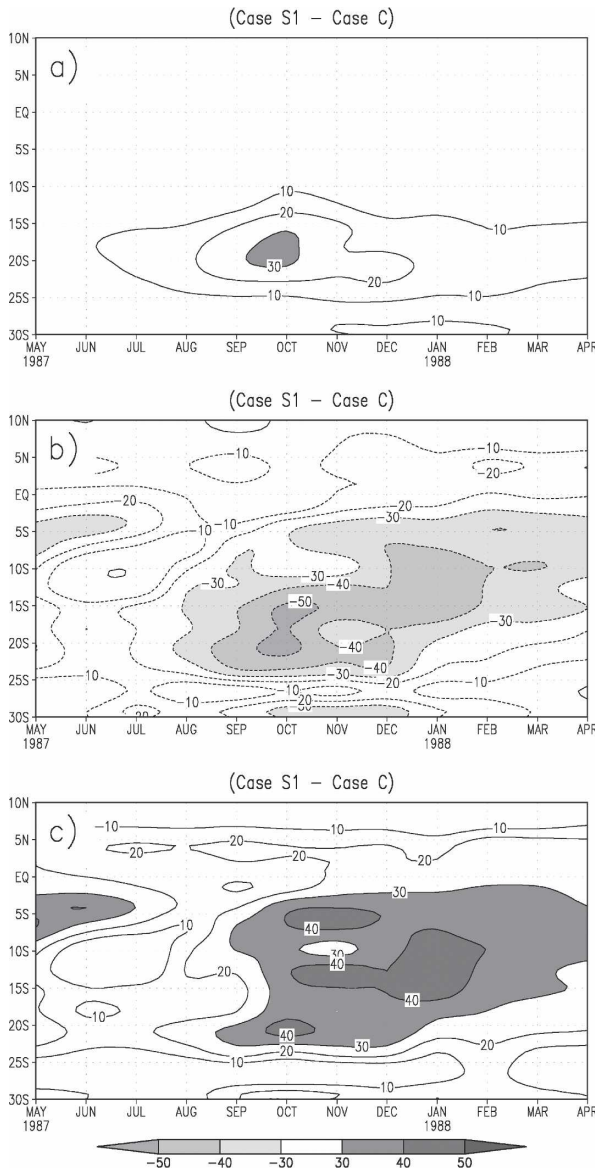
FIG. 5. Temporal evolution of the monthly mean differences between case S1 and case C averaged over 40°–60°W from May 1987 through April 1988: (a) longwave upward, (b) latent heat flux, and (c) sensible heat flux (W m^{-2}).

tive bias to the south). In addition, there was a dry bias along the east side of the Andes and a wet bias along the Andes. Case S1 reduced the wet bias over southeastern Brazil, which was the major problem in monsoon development in case C in October, and partially shifted the SACZ southward. Its SACZ position was consistent with observations (Fig. 6b). Meanwhile, the precipitation over the Amazon and surrounding areas was also reduced. All of these differences are significant at more than a 90% significance level (not shown). Case S1 produced less evaporation than case C in many

areas (Fig. 6c). The spatial distribution of the differences between case S1 and case C, however, were not always consistent with the changes in precipitation. For example, the precipitation was actually increased south of 25°S, in contrast to the changes in evaporation. A comparison between Fig. 1 and Fig. 6c clearly shows that the area with major evaporation reduction was mainly over the savannah region, indicating that the evaporation reductions in case S1 were highly related to the energy partitioning modulated by surface VBP rather than a simple response to changes in precipitation. Case S1 simulated higher sensible heat flux than case C over most parts of the continent, with highest sensible heat flux over the savanna (Fig. 6d), corresponding to reductions in latent heat flux.

Among the vegetation processes, seasonality may contribute substantially to the highest reduction of latent heat flux in the savanna area. In the SSiB model, land surface properties were specified according to vegetation cover types. A parameter set for each of the vegetation types was used based on a variety of sources (Dorman and Sellers 1989; Xue et al. 2001). Seasonally varying monthly values of some vegetation properties, such as LAI, green leaf fraction, and surface roughness length, were prescribed for most vegetation types or calculated in the model for the crop type (Xue et al. 1996b). Savanna had the highest LAI (5.2) in February and gradually decreased in the following months. It had the lowest LAI (1.2) in October and November after the dry season, which was consistent with the satellite-derived International Satellite Land Surface Climatology Project Initiative II (ISLSCP II) LAI (H.-S. Kang et al. 2005, manuscript submitted to *J. Climate*). This lowest LAI was coincident with the large increase in sensible heat flux and decrease in latent heat flux starting in October (Fig. 5c), which had a profound impact on low-level atmospheric circulation.

In October, the SAMS circulation is strongly controlled by equatorial dynamics (Zhou and Lau 1998). Moisture was transferred by southeasterly flow from the Atlantic (Fig. 7a). The SAMS onset was led by a southward reversal of the cross-equatorial flow (Wang and Fu 2002). The southeasterly airflow from the Atlantic moved into the continent and turned counterclockwise, moving southward along the lee side of the Andes. Xue et al. (2004) found that during the early monsoon stage, the heating produced by VBP helped the circulation turn over the east Asian and African continents due to the geostrophic balance. Without this heating, the wind flow would move straight forward without turning (Xue 2005). However, this difference in circulation disappeared during the monsoon mature stage when convective activity dominates heating. We
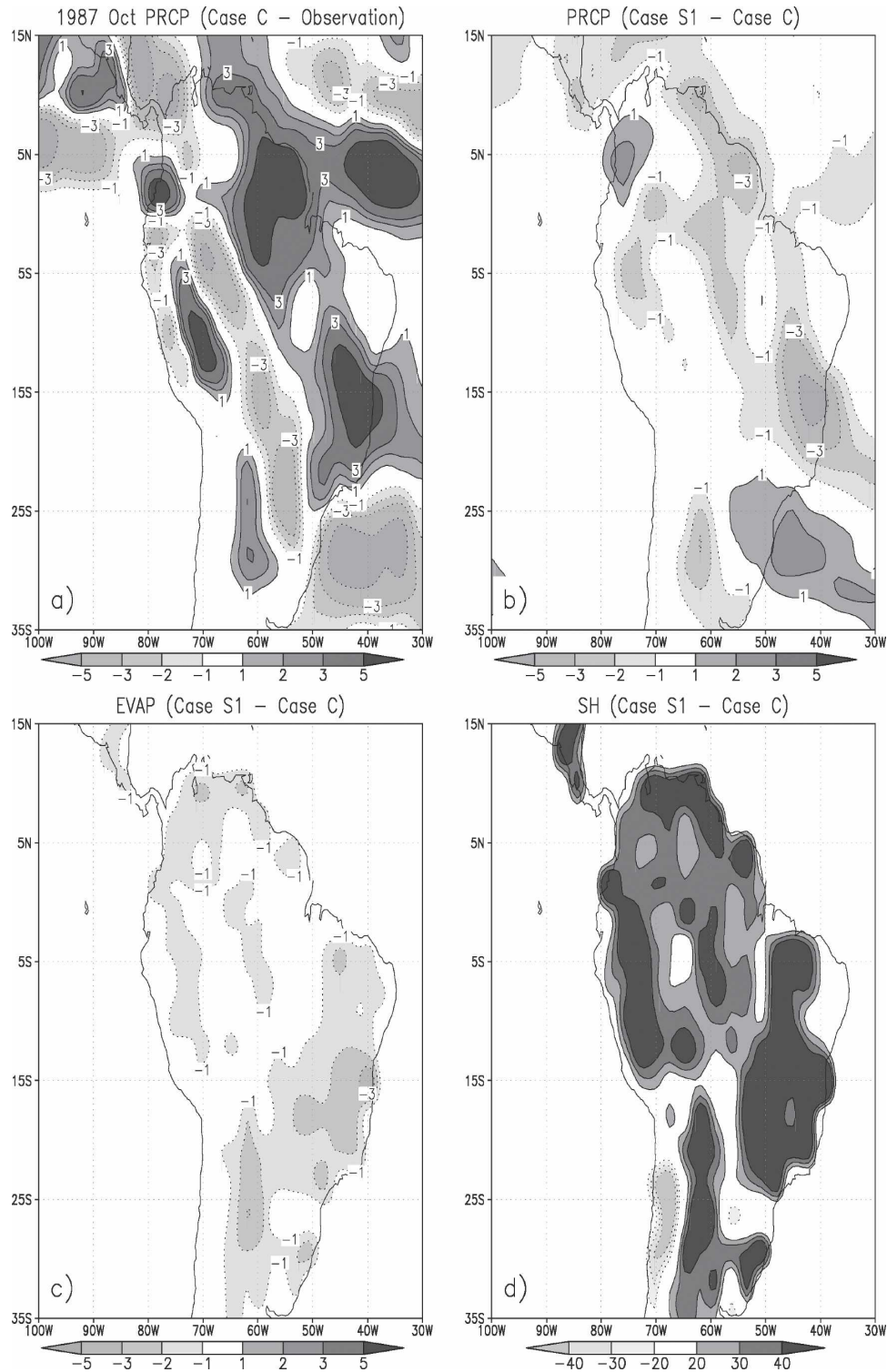
FIG. 6. October precipitation differences (mm day^{-1}): (a) between case C and CMAP and (b) between case S1 and case C. October differences between case S1 and case C: (c) evaporation (mm day^{-1}) and (d) sensible heat flux (W m^{-2}).
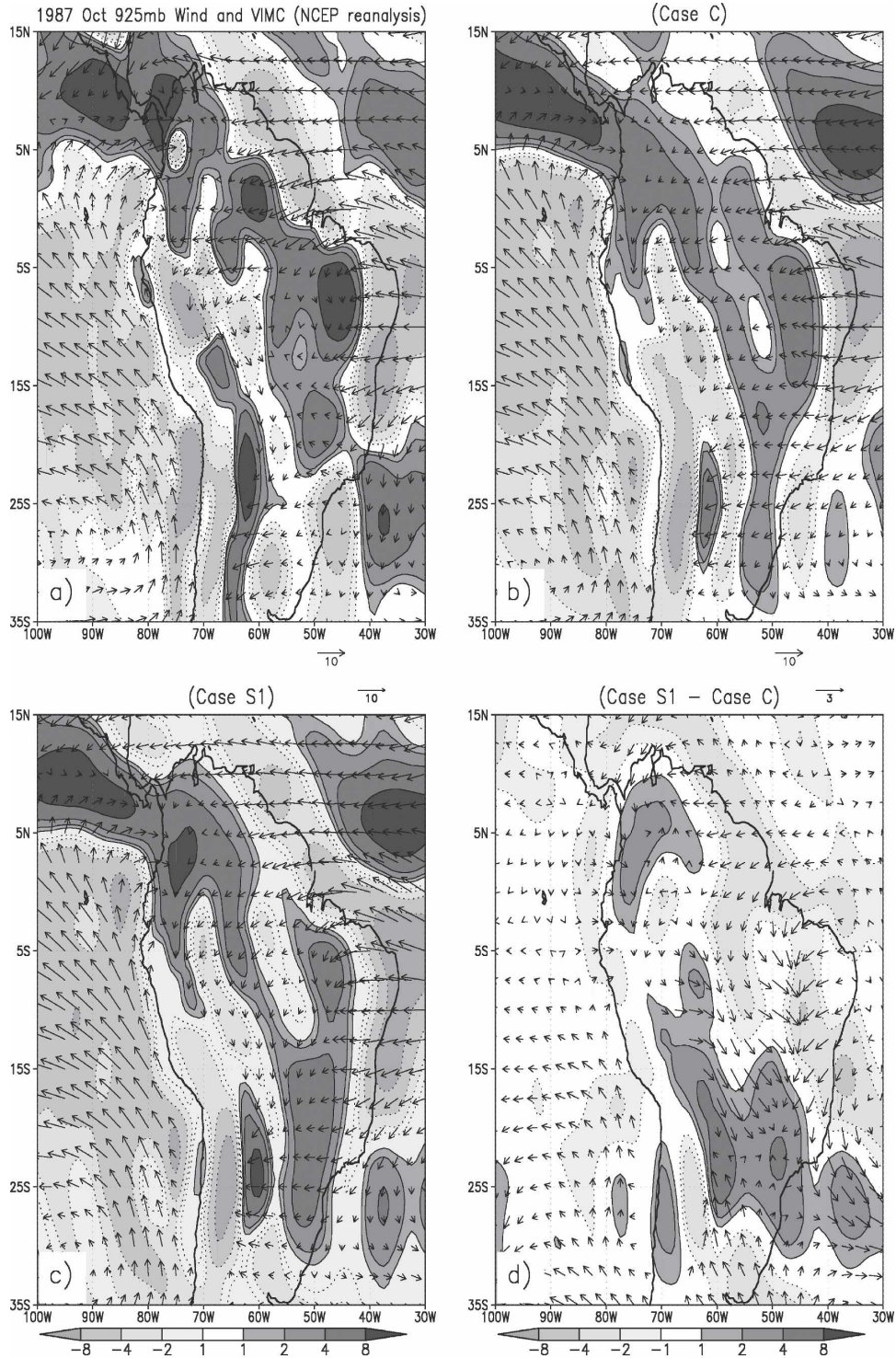
FIG. 7. October 1987 925-hPa wind field (m s^{-1}) and vertical integrated moisture flux convergence (mm day^{-1}): (a) reanalysis, (b) case C, (c) case S1, and (d) case S1 − case C.

found a similar situation in this study. In austral spring, the trade winds from the Atlantic turn counterclockwise while crossing northern South America, as discussed earlier. This turning was weaker in case C than in reanalysis or case S1 (Figs. 7b–d). In case C, there was not any turning in September (not shown) and only a weak turning in October (Fig. 7b), which indicated that the orography alone in the NCEP GCM was not sufficient to produce the observed turning. The turning in case S1 was much stronger and produced a relative anticyclone anomaly (compared to case C) in both September (not shown) and October (Figs. 7c and 7d). It is important to understand the cause of the forming of this anticyclone. The northern branch of this anticyclone created anomalous dry advection and reduced convection over northern South America between 5°N and 5°S, while its southern branch induced anomalous moist convergence between 20° and 30°S and shifted the SACZ to the south. Near the equator, where the Coriolis forcing was weak, the cause of the forming of this circulation change should be different from that over the eastern Asian continent.

Several studies have explored the mechanisms that affect the SAMS development. Rodwell and Hoskins (2001) found that the Rossby wave response to the west of subtropical monsoon heating, interacting with the midlatitude westerlies, produces a region of adiabatic descent, which may contribute to the Mediterranean-type climates of regions such as Chile. Zhou and Lau (1998) found that sensible versus latent heating over the highland was bound to play an important role in the evolution of the 1989–90 SAMS. The importance of moisture flux convergence (MFC) and the thermal low in South American precipitation was also found in perpetual January GCM experiments (Lenters and Cook 1995). Furthermore, it has been found that the ventilation effect [i.e., the import into South America of low moist static energy (MSE) air from the cool ocean (primarily Pacific) or the export of high MSE out of the continent] had a very strong impact on the extent of the rain zone and limited the southward extent of the SAMS (Chou and Neelin 2001). Chou and Neelin (2003) also indicated that the horizontal advection of MSE (AMSE) had very important effects on vertical motion and low-level convergence, and then MFC, in convective regions.

Figure 8 shows the vertical integrated AMSE difference from the surface to 500 mb between case S1 and case C in October. Similar to Chou and Neelin (2001), the vertical integrated AMSE is defined as

$$-(1/g)\int \mathbf{V} \cdot \boldsymbol{\nabla}(C_P T + gz + L_c w)\, dP, \qquad (1)$$
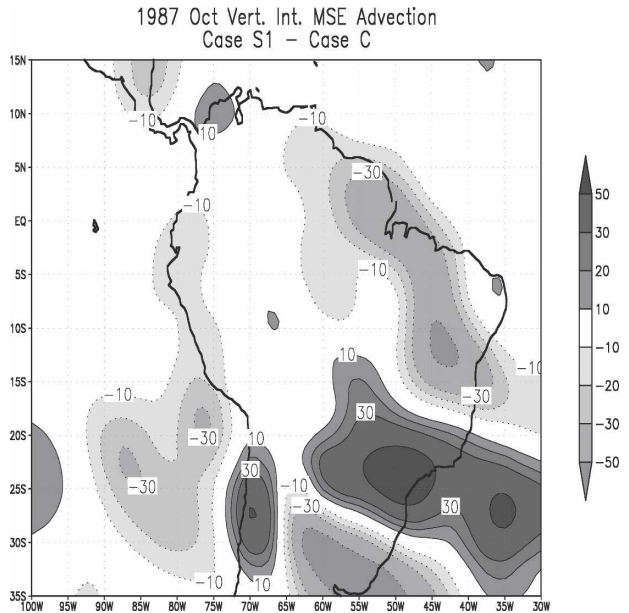

FIG. 8. October 1987 vertically integrated AMSE difference from surface to 500 mb between case S1 and case C (W m^{-2}).

where C_p is specific heat of dry air at constant pressure, T is air temperature (K), g is gravity acceleration (m s^{-2}), z is height (m), L_c is latent heat of condensation (J kg^{-1}), w is water vapor mixing ratio, and $\mathbf{V}$ is horizontal wind vector. The temperature in southeast Brazil was about 4° and 2°C higher at the surface and 925 mb, respectively, in case S1 than in case C (not shown), consistent with the high sensible heat flux in case S1 (Fig. 6d). The strong easterly winds and warming in case S1 over the continent generated stronger negative AMSE between 10° and 20°N along the northeastern coast (Fig. 8), which intensified the ventilation effect caused by a low MSE oceanic air mass. Ventilation tends to have a cooling and drying effect in the atmospheric column. The reduced MSE induced sinking (not shown) and contributed to anticyclonic airflow over the area. The relative anticyclone around 15°–20°S, 35°–40°W was consistent with the relative divergence zone (Fig. 7d), which corrected the positive bias of precipitation obtained in case C in that area. These results indicate that modulation of the heating gradient over the South American continent in October has a substantial implication on the development and extent of the monsoon onset. Furthermore, the stronger southward airflow along the eastern slope of the Andes in case S1 brought unstable and high MSE air from the Amazon and met northward flow near 25°S, generating positive AMSE (Fig. 8) and an intense convergence area over that region (Fig. 7d), which shifted the SACZ southward (see the dipole difference pattern between

10° and 30°S in Fig. 6b). The results in this study reveal that, in addition to the gradient between the Pacific and the South American continent as shown in Chou and Neelin (2001), temperature and heating gradients between the continent and the Atlantic induced by VBP also affect the monsoon evolution. In addition, geostrophic adjustment near 20°S seems to also contribute to this convergence (Fig. 7d).

We also note that there is positive integrated AMSE on the southwestern coast of South American (Fig. 8) and a relative convergence (Fig. 7d) and a rising motion in this area at 850 mb (not shown). Rodwell and Hoskins (2001) have indicated that the reduced monsoon convection could weaken the associated Rossby wave subsidence to its southwest. Our results are in agreement with this concept, and less monsoon precipitation in the Amazon (Fig. 6a) was associated with a positive AMSE and a relative stronger convergence at the southwest coast area.

The precipitation (evaporation) over continental South America for case S1 (case C) are 107 (136) and 81 (116) mm day^{-1}, respectively. The evaporation provided a large contribution to continental precipitation in October. The evaporation difference between case S1 and case C in October was 35 mm month^{-1}, which was more than the reduction of precipitation, 29 mm month^{-1}. This indicates that the difference in local evaporation between case S1 and case C dominated the changes in atmospheric moisture for the whole continent. However, Figs. 6b and 7d indicate that spatial distribution of the precipitation difference (Fig. 6b) was consistent with the changes in MFC (Fig. 7d), not in evaporation (Fig. 6c). Therefore, it seems that the dynamical processes indicated by AMSE (Fig. 8) in the low-level atmosphere and VBP at the surface modulated the impact of evaporation change on the spatial distribution of precipitation.

In December, the northward monsoon movement in case C was too fast and merged with the ITCZ too early (Figs. 3g, 3h, and 4b), which produced a dipole anomaly pattern: strong positive bias in precipitation in the northeast part of South America and negative bias to its southwest (Fig. 9a). The SACZ was associated with southeasterly flow over the eastern Atlantic, and it was too strong and shifted to the north in case C as in October. Case S1 partially corrected the unrealistic merging between SAMS precipitation and the ITCZ and shifted the SACZ back to the south (Fig. 9b). Similar to the October case, all these differences were significant at the 90% level.

Compared with October, the area with major precipitation reduction moved northeast (Figs. 6b and 9b). The northeast Brazilian shrub area (Fig. 1) became one

of the areas with major precipitation and evaporation reductions in December (Figs. 9b and 9c). Shrubs had the highest LAI in March (1.5) and lowest LAI in November and December (0.25). As described earlier, the seasonality of savanna and shrubs was from our standard table (Dorman and Sellers 1989). Evaporation contributed to the changes in precipitation, in particular in the shrub area (Fig. 9c). The precipitation and evaporation reductions over the continent were 26 and 36 mm month^{-1}, respectively. The corresponding values over the area between 15°S and 5°N, 70° and 35°W, where precipitation had the most reduction, were 49 and 36 mm month^{-1}, respectively. However, the spatial pattern of changes in evaporation did not correspond to the changes in precipitation over many areas. In the SACZ area, the changes in these two variables had the opposite signs. Similar to the October situation, ventilation in December also played a role for these changes, although not as strong as in October (not shown). The spatial distribution of the changes in the vertical integrated moisture flux divergence was consistent with changes in precipitation (Figs. 9b and 10d). Circulation changes played an important role in modulating the spatial distribution of atmospheric moisture.

A comparison between reanalysis data and the simulation clearly shows that the simulated airflow and moisture flux convergence in case S1 are closer to reanalysis than in case C. For example, case S1 simulated a convergence maximum around 5°–15°S, 45°W and a divergence center to its east (Fig. 10c), consistent with the reanalysis (Fig. 10b). Convergence and divergence centers in case C were both very weak. The northerly wind flow along the eastern scarp of the Andes in case S1 was stronger and was also closer to reanalysis than for case C (Figs. 10c and 10d). A comparison between the difference in moisture flux convergence between case S1 and case C shows important differences between October and December in some regions. For instance, the area with the maximum sensible heat difference between cases S1 and C was mainly located over the northeast corner of Brazil, a shrubland, in December (Fig. 9d). The area with major reduction in vertically integrated MSE (not shown), major convergence difference, and major precipitation reduction therefore also moved to that area and the nearby Atlantic Ocean (Figs. 9b and 10d), which contributed to correcting the strong northward mergence of SAMS with the ITCZ in case C. The strong divergence likely induced a strong convergence to its west, around 5°–10°S, 45°W (Fig. 10d), consistent with reanalysis (Fig. 10a). In addition, strong northerly flow in case S1 may contribute to an intensive SACZ (Fig. 10d) as shown in October. Because the differences in surface energy partitioning,
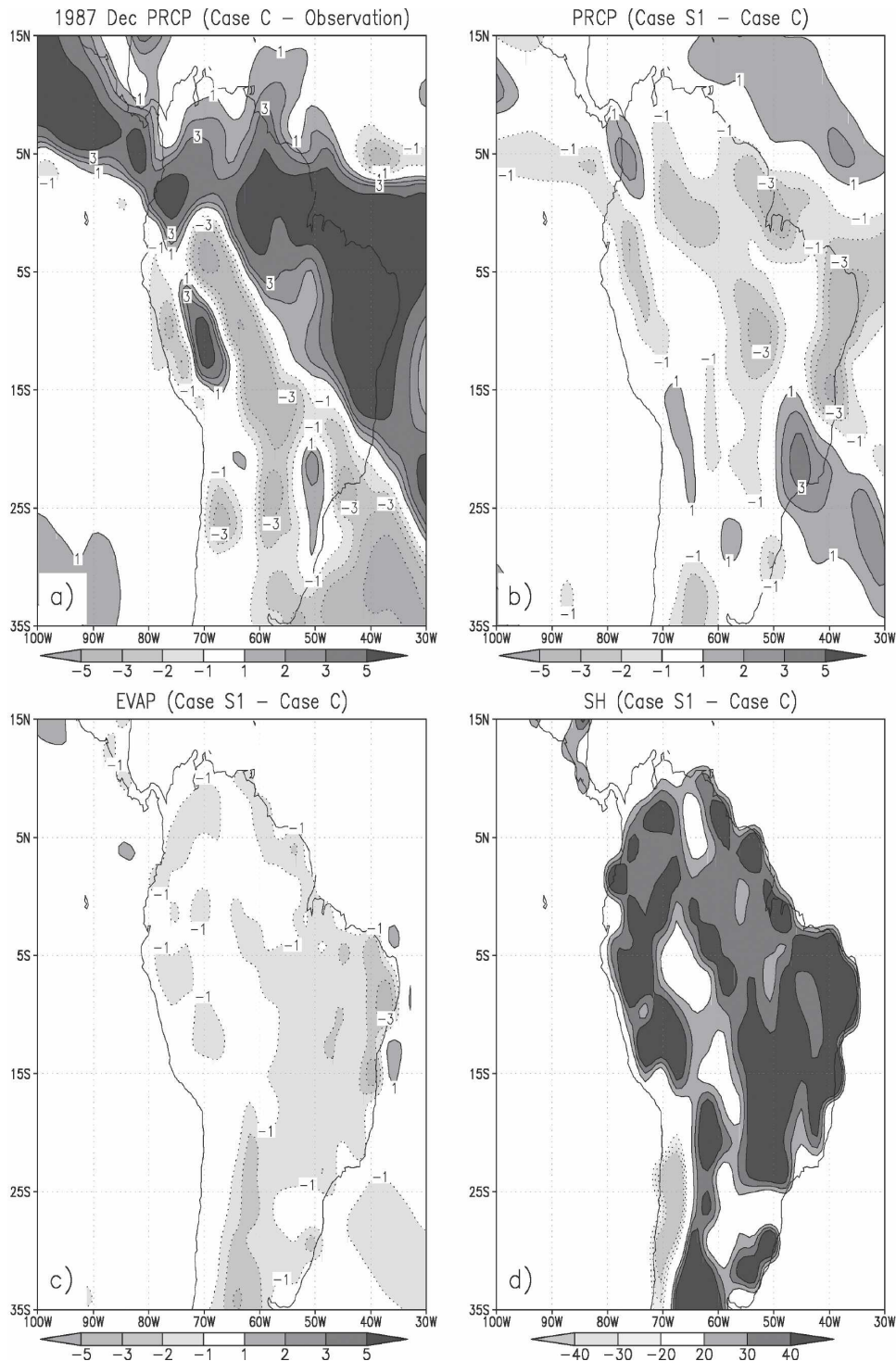
FIG. 9. As in Fig. 6 but for December.

low-level circulation, and MFC discussed for December persisted during the entire rainy season, the DJF precipitation difference over the South American continent was very similar to December (Figs. 2d and 9b).

An important feature in SAMS is the Bolivian high during the monsoon mature stage. Previous theoretical and diagnostic studies indicated that the high was generated by remote forcing from Africa and local forcing
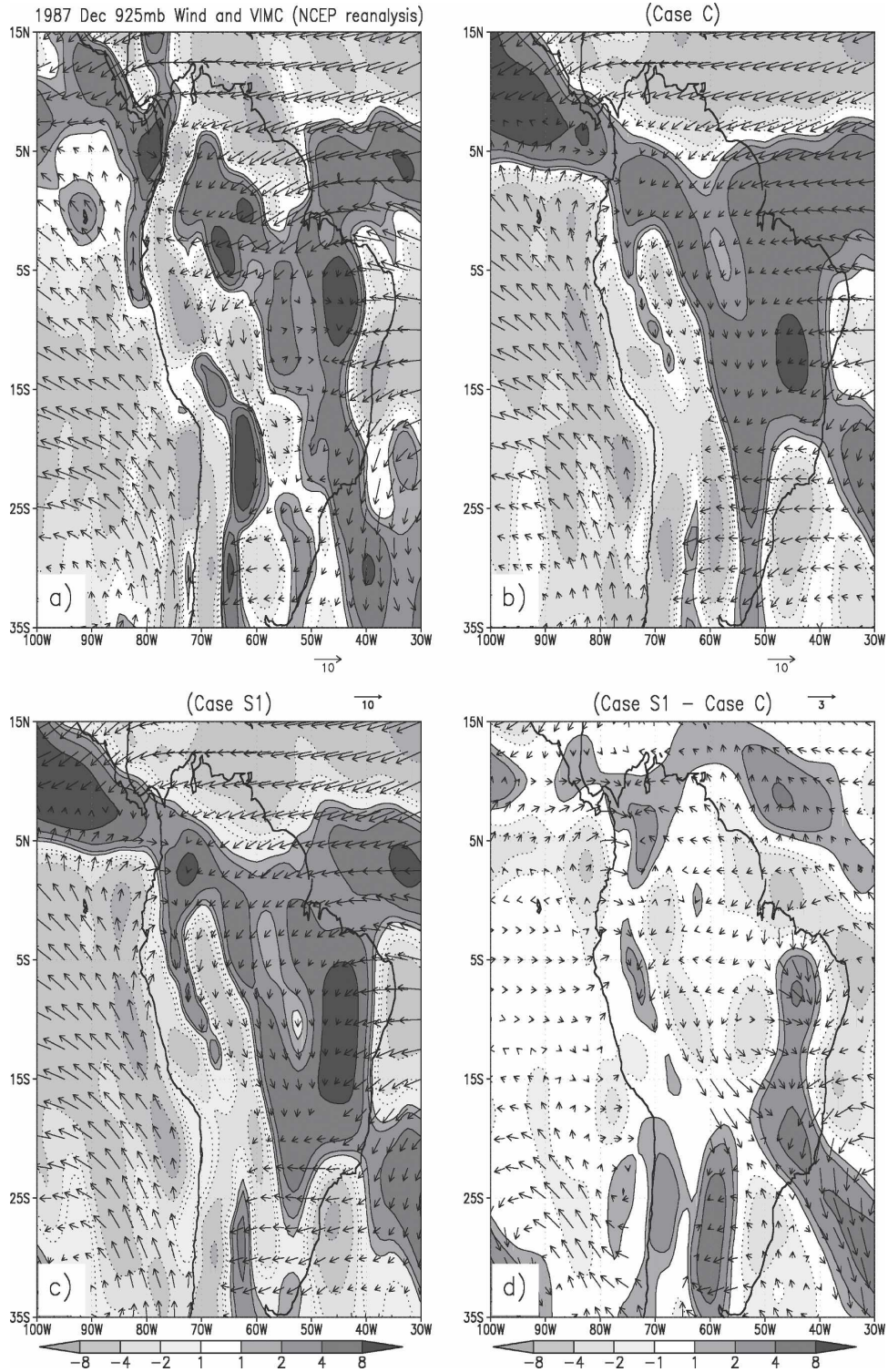
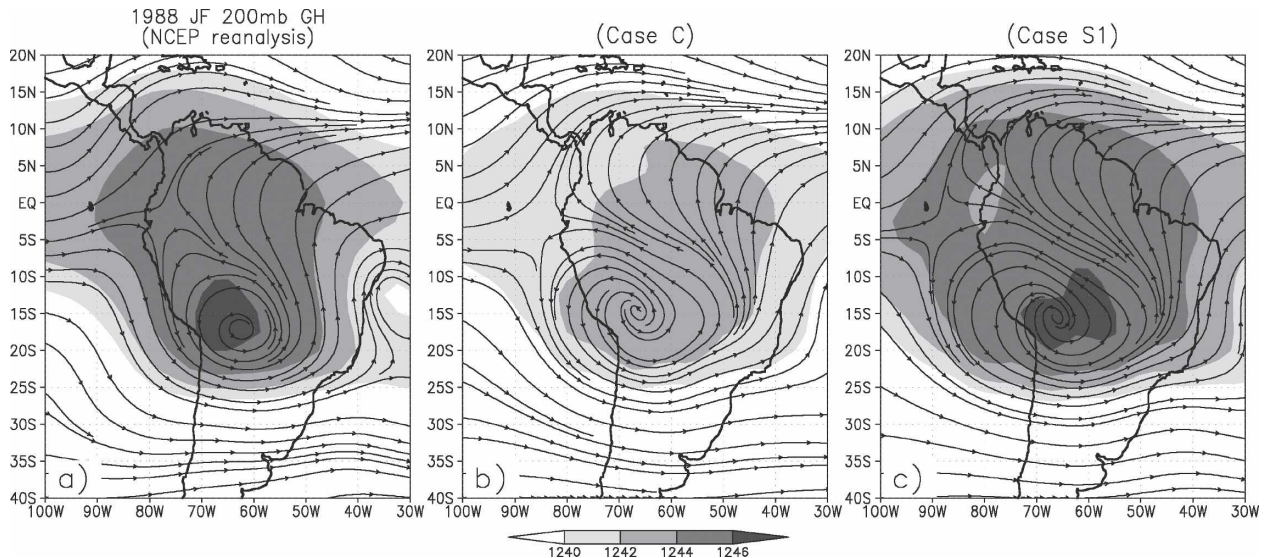FIG. 10. As in Fig. 7 but for December.

FIG. 11. January–February 1988 geopotential height (10 gpm) and streamlines at 200 hPa: (a) reanalysis, (b) case C, and (c) case S1.

over South America, including condensational heating over the Amazon (e.g., Lenters 1997; Nogués-Paegle et al. 2002; among many others). This high pressure system was formed in January and February in 1987 (Fig. 11a) and corresponded very well to the thermal low near the surface in this study, as evident in Fig. 9d. With strong thermal heating at the land surface, the Bolivian high was better simulated in case S1 (Fig. 11), which demonstrates the effect of local sensible forcing due to VBP on its formation.

5. Discussions and summary

This study explored the impact of land surface processes on the structure and evolution of the SAMS with an emphasis on the evolution of precipitation. The results were obtained using the NCEP GCM coupled with two different land surface parameterizations; one includes an explicit representation of vegetation processes in the calculation of surface fluxes, while the other does not. The simulations consisted of five pairs of 1-yr integrations differing in the initial conditions for the atmosphere but with the same soil moisture to examine the impact of VBP on SAMS and to evaluate the robustness of the model results.

This research is a further investigation of the role and mechanisms of VBP in view of Sato et al.'s (1989) study. Although the results obtained with the two different parameterizations were compared with each other and with observations, our goal was principally to better understand the influence of VBP on the pro-

cesses of monsoon development. Our results show that, during the austral summer, the GCM with and without explicit vegetation processes produced similar monthly mean simulations of precipitation at the planetary scale when similar monthly mean surface albedo and initial soil moisture were used (Fig. 2). However, at the continental and synoptic scales, more complete representation of land surface processes produced a simulation of the SAMS that is closer to observations. The effects were mainly manifested in the temporal evolution of the monsoon, its strength, the spatial distribution of precipitation, and associated circulation at continental and synoptic scales. GCM/Soil correctly produced a South American rainy season. The process of southward movement of precipitation in October, however, was not clearly defined. The merging of SAMS with the ITCZ was too early and too strong, producing a very wet rainy season. GCM/SSiB improved the simulations in all these aspects, as well as in the values of monthly mean precipitation. The improvement in the simulation associated with VBP was consistent throughout the entire year (Table 1). These differences could have significant implications for regional water resources, as shown in Figs. 6b and 9b. All these findings are also consistent with our boreal summer monsoon study (Xue et al. 2004).

It could be argued that the deficiencies in case C could be reduced by modification of the GCM/Soil parameterization, such as changing the number of soil layers, soil depths, or cleverly tuning the values of soil conductivity, etc. In fact, after Sato et al.'s (1989) study

a similar argument attributed the deficiency in GCM/ Bucket to the improper specification of the beta parameter in the GCM. However, several more recent studies such as the Project for Intercomparison of Land surface Parameterization Schemes (PILPS: Henderson-Sellers et al. 1993) have consistently shown better simulations in surface water and energy budgets by introducing biophysical models. Most major contemporary GCMs currently include a biophysical submodel for their surface processes. In this study, as a matter of fact, both the soil model in the NCEP GCM and SSiB soil submodel apply diffusion equations for soil moisture transfer and the Paulson equation for calculation of surface layer aerodynamic resistance, although SSiB modifies it for vegetation-covered conditions. The GCM/Soil has been thoroughly tested and evaluated for numerical weather forecasting and reanalyses, and produced reasonable climate mean results. It is unlikely that any tuning of the GCM/Soil for different Bowen ratios for one case would not be at the expense of a better simulation of its mean climate. Both the NCEP soil submodel and SSiB are physically based models, which was made evident by the lack of any need for tuning when the soil model was replaced with SSiB. The differences between the simulations by the two models could be clearly related to physical and dynamic processes even in a complex GCM system. We believe that this and our other studies (e.g., Xue et al. 2004) strongly suggest that the VBP is a major contributor to the difference in the simulation of intraseasonal monsoon evolution. We also believe more experiments with different models and different approaches are necessary to further tackle this issue.

To understand the effect of soil moisture variability on surface water and energy balances and land–atmosphere interaction, we also used GSWP soil moisture for a test (case S2). GSWP (Dirmeyer et al. 1999) is a pilot study intended to produce a soil wetness global dataset by using 1987 and 1988 meteorological observations and analyses to drive land surface models. SSiB has participated in this project. This project is intended to produce "better" soil moisture fields for GCM application. In general, the soil in GSWP was drier than that in the reanalysis data over South America (Figs. 12a–c), although the difference at the rooting zone was dramatically reduced after one month's simulation (Fig. 12d). This reduction indicates that the model adjusted the soil moisture to its climatology very quickly. After the soil moisture was modified by monsoon precipitation, both case S1 and case S2 had virtually the same soil moisture in the rooting zone during the rainy season (not shown). The monthly mean precipitation obtained in case S2 is also listed in Table 1. The improvement of the precipitation simulation in South

America in case S2 was not as substantial as in our East Asian study (Xue et al. 2004) since case S1 was already closer to observations. In addition, in the East Asian study, the initial starting date (1 May) was much closer to the monsoon onset (late May); therefore, proper initial soil moisture had a larger impact on the monsoon simulation. However, although the soil moisture differences between cases S2 and S1 during the rainy season were very small, the difference in precipitation was still large in February and March (Table 1), especially in Brazil (not shown), which was an indication that the effect of soil moisture lasted longer. Further comprehensive investigations regarding soil moisture effects are required.

This study confirms that different partitioning of latent heat and sensible heat fluxes (i.e., different Bowen ratio) caused different latitudinal and longitudinal thermal gradients at the surface. Case S1 produced more sensible heat flux, especially during October–January, which helped to produce a stronger heat gradient between continent and ocean. Ventilation effects contributed to a stronger counterclockwise turning of the low-level wind from the Atlantic Ocean toward the continent during the premonsoon and early monsoon stages. Furthermore, it was identified that the seasonality of savanna and shrublands to the south and east of the Amazon rain forest influenced circulation and contributed to a relative anticyclone anomaly, which prevented the monsoon from moving into southeast Brazil at monsoon onset and an overly strong northward mergence of SAMS with the ITCZ at the early monsoon mature stage.

Land surface processes modulate the surface water and energy balance, which in turn affect land–atmosphere interactions that are complex and nonlinear. The dominant interaction mechanisms depend on temporal and spatial scales, topographic features, and background climate conditions (e.g., Xue 1996; Xue et al. 2001, 2004). In this study, evaporation and MFC play important but seemingly different roles in modulating the changes in simulations with/without vegetation processes. Evaporation and subsequent latent heat release play important roles in SAMS development (e.g., Zhou and Lau 1998). Monthly mean evaporation rates for case S1 and case C over the South American continent are listed in Table 1. The ratios of annual mean evaporation to precipitation over South America were 68% and 81% in case S1 and case C, respectively. The Amazon rain forest area contributed 57.2% and 50.1% of total evaporation over the South American continent. The January–March (JFM) mean ratios of evaporation to precipitation were 55% and 69% in case S1 and case C, respectively. The percentages are much lower than
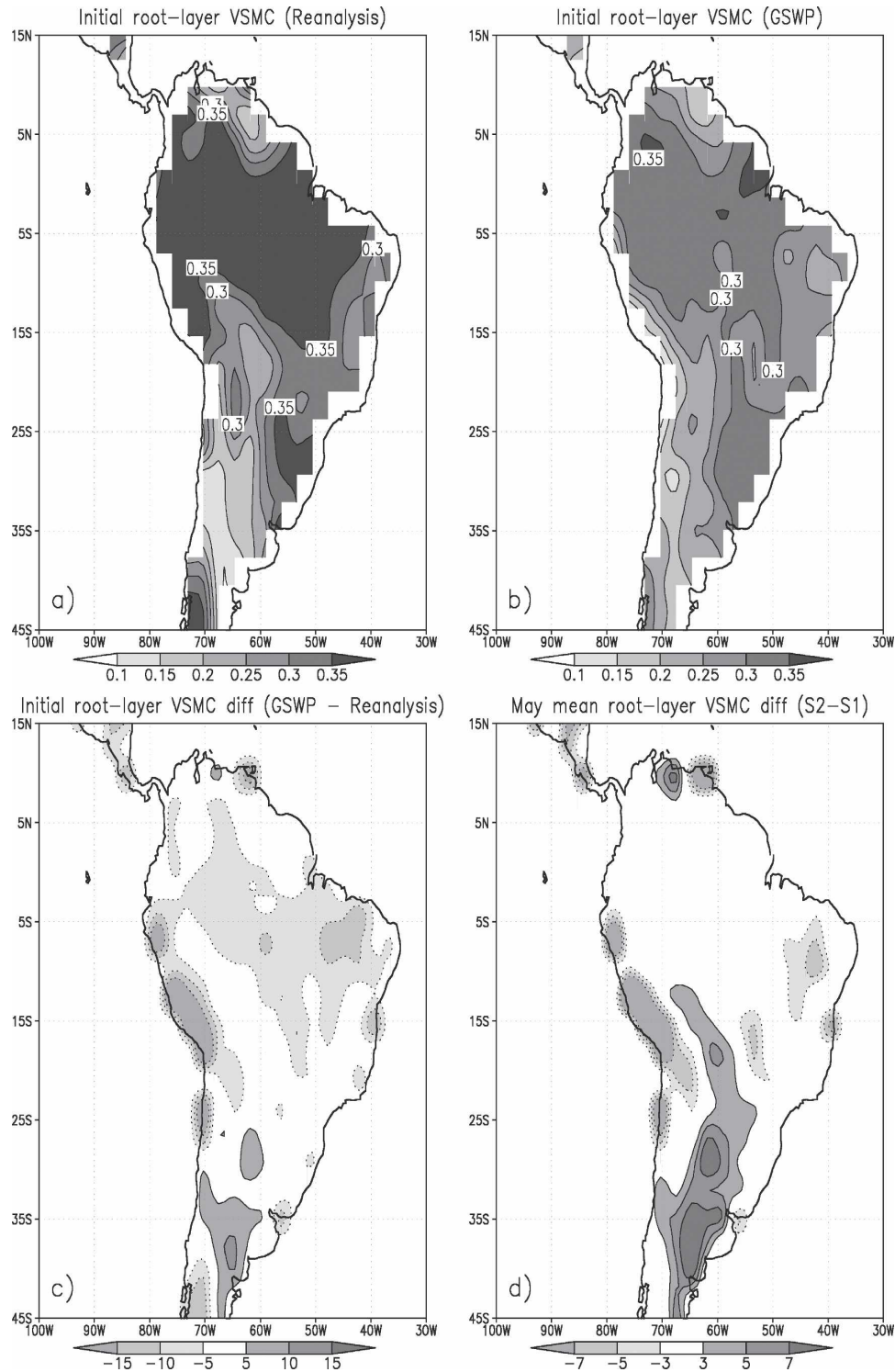
FIG. 12. Initial volumetric soil water content for (a) reanalysis, (b) GSWP, and (c) GSWP − reanalysis; (d) May mean soil moisture difference between case S2 and case S1 at rooting zone.

TABLE 2. Mean precipitation and evaporation differences between case S1 and case C over the South American continent (mm month^{-1}).

	Precipitation	Evaporation
Annual	−13.9	−27.6
Jan	−18.6	−32.9
Feb	−7.0	−30.8
Mar	−7.5	−28.4
Apr	−3.7	−24.0
May	−20.1	−26.2
Jun	−8.4	−25.9
Jul	−3.0	−17.3
Aug	−2.8	−20.7
Sep	−17.0	−28.8
Oct	−28.8	−34.7
Nov	−23.1	−34.5
Dec	−25.7	−36.4

the annual mean, which indicates that the moisture flux transport from the Atlantic plays an important role in summer monsoon precipitation. In this study the greatest atmospheric moisture difference over the continent between case S1 and case C was caused by the evaporation difference between these two cases (Table 2). On the other hand, the spatial distribution of changes in precipitation was mainly determined by changes in AMSE and MFC, as discussed earlier. This indicates that VBP modulated the surface water budget. But its impact on precipitation was mainly controlled by the changes in circulation after changes in the heat gradient, consistent with the fundamental monsoon physics; that is, the monsoon itself is considered to be an inevitable consequence of land–sea contrasts in sensible heating (Rodwell and Hoskins 2001). This study also shows that changes in SALLJ and circulation near the South American east coast, which were affected by the heating gradient between the Atlantic and the continent, played an important role in modulating the SAMS development.

This is a case study using the NCEP GCM. To confirm the findings and hypothesis in this study, more case studies with different models are necessary. This study also shows that accurate simulations and predictions of SAMS are a formidable task and that crucial improvements remain to be made. We have identified the possible importance of the seasonality of savanna and shrubs in the SAMS development. Although the specified LAI values in the dry season we used were consistent with the satellite-derived data, the LAI values (4–5) in the wet season were much higher than those produced by remotely sensing methods (about 3) (H.-S. Kang et al. 2005, manuscript submitted to *J. Climate*), which may have contributed to the wet bias in case S1

in the wet season. More realistic specifications of savanna seasonality based on ground truth measurements and remote sensing, as well as applications of dynamic vegetation models, should be very useful in further assessing the role of vegetation seasonality in SAMS.

REFERENCES

Berbery, E. H., and V. R. Barros, 2002: The hydrological cycle of the La Plata Basin in South America. *J. Hydrometeor.,* **3,** 630–645.

Budyko, M. I., 1974: *Climate and Life.* Academic Press, 508 pp.

Businger, J. A., J. C. Wyngaard, Y. Izumi, and E. G. Bradley, 1971: Flux–profile relationships in the atmospheric surface layer. *J. Atmos. Sci.,* **28,** 181–189.

Cavalcanti, I. F. A., and Coauthors, 2002: Global climatological features in a simulation using the CPTEC–COLA AGCM. *J. Climate,* **15,** 2965–2988.

Charney, J., W. J. Quirk, S.-H. Chow, and J. Kornfield, 1977: A comparative study of the effects of albedo change on drought in semi-arid regions. *J. Atmos. Sci.,* **34,** 1366–1385.

Chou, C., and J. D. Neelin, 2001: Mechanisms limiting the southward extent of the South American summer monsoon. *Geophys. Res. Lett.,* **28,** 2433–2436.

——, and ——, 2003: Mechanisms limiting the northward extent of the northern summer monsoons over North America, Asia, and Africa. *J. Climate,* **16,** 406–425.

Chou, M.-D., 1992: A solar radiation model for use in climate studies. *J. Atmos. Sci.,* **49,** 762–772.

——, and M. J. Suarez, 1994: An efficient thermal infrared radiation parameterization for use in general circulation models. Series on Global Modeling and Data Assimilation, NASA Tech. Memo. TM-1994-104606, 85 pp.

Dickinson, R. E., and A. Henderson-Sellers, 1988: Modeling tropical deforestation: A study of GCM land-surface parameterizations. *Quart. J. Roy. Meteor. Soc.,* **114,** 439–462.

Dirmeyer, P. A., A. J. Dolman, and N. Sato, 1999: The pilot phase of the Global Soil Wetness Project. *Bull. Amer. Meteor. Soc.,* **80,** 851–878.

Dorman, J. L., and P. Sellers, 1989: A global climatology of albedo, roughness length and stomatal resistance for atmospheric general circulation models as represented by the Simple Biosphere Model (SiB). *J. Appl. Meteor.,* **28,** 833–855.

Eltahir, E. A. B., and R. L. Bras, 1993: Spatial distribution of precipitation recycling in the Amazon basin. *The World at Risk: Natural Hazards and Climate Change*, R. L. Bras, Ed., American Institute of Physics, 174–179.

Fu, R., R. E. Dickinson, M. Chen, and H. Wang, 2001: How do tropical sea surface temperatures influence the seasonal distribution of precipitation in the equatorial Amazon? *J. Climate,* **14,** 4003–4026.

Grimm, A. M., 2000: Climate variability in southern South America associated with El Niño and La Niña events. *J. Climate,* **13,** 35–58.

Hansen, M. C., R. S. DeFries, J. R. G. Townshend, and R. Sohlberg, 2000: Global land cover classification at 1 km spatial resolution using a classification tree approach. *Int. J. Remote Sens.,* **21,** 1303–1330.

Hastenrath, S., and L. Heller, 1977: Dynamics of climate hazards in Northeast Brazil. *Quart. J. Roy. Meteor. Soc.,* **103,** 77–92.

Henderson-Sellers, A., and A. J. Pitman, 2002: Comments on suppressing impacts of the Amazonian deforestation by the global circulation change. *Bull. Amer. Meteor. Soc.,* **83,** 1657–1661.

——, Z.-L. Yang, and R. E. Dickinson, 1993: The project for intercomparison of land-surface parameterization schemes. *Bull. Amer. Meteor. Soc.,* **74,** 1335–1349.

Hong, S.-Y., and H.-L. Pan, 1996: Nonlocal boundary layer vertical diffusion in a medium-range forecast model. *Mon. Wea. Rev.,* **124,** 2322–2339.

Kalnay, E., M. Kanamitsu, and W. E. Baker, 1990: Global numerical weather prediction at the National Meteorological Center. *Bull. Amer. Meteor. Soc.,* **71,** 1410–1428.

——, and Coauthors, 1996: The NCEP/NCAR 40-Year Reanalysis Project. *Bull. Amer. Meteor. Soc.,* **77,** 437–471.

Kanamitsu, M., and Coauthors, 2002: NCEP dynamical seasonal forecasting system 2002. *Bull. Amer. Meteor. Soc.,* **83,** 1019–1037.

Kistler, R., and Coauthors, 2001: The NCEP–NCAR 50-year reanalysis: Monthly means CD-ROM and documentation. *Bull. Amer. Meteor. Soc.,* **82,** 247–267.

Kousky, V. E., M. T. Kagano, and I. F. A. Cavalcanti, 1984: A review of the Southern Oscillation: Oceanic–atmospheric circulation changes and related rainfall anomalies. *Tellus,* **36A,** 490–504.

Lau, K.-M., and J. Zhou, 2003: Responses of the South American summer monsoon climate system to ENSO during 1997–1999. *Int. J. Climatol.,* **23,** 529–539.

Lenters, J. D., 1997: On the origin of the Bolivian high and related circulation features of the South American climate. *J. Atmos. Sci.,* **54,** 656–677.

——, and K. H. Cook, 1995: Simulation and diagnosis of the regional summertime precipitation climatology of South America. *J. Climate,* **8,** 2988–3005.

Marengo, J. A., B. Leibmann, V. E. Kousky, N. P. Filizola, and I. C. Wainer, 2001: Onset and end of the rainy season in the Brazilian Amazon basin. *J. Climate,* **14,** 833–852.

Mechoso, C., and G. Perez-Iribarren, 1992: Streamflow in southeastern South America and the Southern Oscillation. *J. Climate,* **5,** 1535–1539.

Miyakoda, K., and J. Sirutis, 1986: Manual of the E-physics. Geophysical Fluid Dynamics Laboratory, Princeton University, 122 pp.

Moorthi, S., and M. J. Suarez, 1992: Relaxed Arakawa–Schubert: A parameterization of moist convection for general circulation models. *Mon. Wea. Rev.,* **120,** 978–1002.

Moura, A. D., and J. Shukla, 1981: On the dynamics of drought in Northeast Brazil: Observation, theory, and numerical experiments with a general circulation model. *J. Atmos. Sci.,* **38,** 2653–2675.

Nobre, C. A., J. Shukla, and P. Sellers, 1991: Amazonian deforestation and regional climate change. *J. Climate,* **4,** 957–988.

Nobre, P., and J. Shukla, 1996: Variations of sea surface temperature, wind stress, and rainfall over the tropical Atlantic and South America. *J. Climate,* **9,** 2464–2479.

Nogués-Paegle, J., and K. C. Mo, 1997: Alternating wet and dry conditions over South America during summer. *Mon. Wea. Rev.,* **125,** 279–291.

——, and Coauthors, 2002: Progress in Pan American CLIVAR Research: Understanding the South American Monsoon. *Meteorologica,* **27,** 3–32.

Pan, H.-L., and L. Mahrt, 1987: Interaction between soil hydrology and boundary layer developments. *Bound.-Layer Meteor.,* **38,** 185–202.

Paulson, C. A., 1970: Mathematical representation of wind speed and temperature profiles in the unstable atmospheric surface layer. *J. Appl. Meteor.,* **9,** 857–861.

Pisciottano, G., A. Diaz, G. Cazes, and C. R. Mechoso, 1994: El Niño–Southern Oscillation impact on rainfall in Uruguay. *J. Climate,* **7,** 1286–1302.

Rao, V. B., S. R. Chapa, and S. H. Franchito, 1999: Decadal variation of atmosphere–ocean interaction in the tropical Atlantic and its relationship to the Northeast Brazil rainfall. *J. Meteor. Soc. Japan,* **77,** 63–75.

Rodwell, M. J., and B. J. Hoskins, 2001: Subtropical anticyclones and summer monsoons. *J. Climate,* **14,** 3192–3211.

Ropelewski, C. F., and M. S. Halpert, 1987: Global and regional scale precipitation patterns associated with the El Niño/Southern Oscillation. *Mon. Wea. Rev.,* **115,** 1606–1626.

Sato, N., P. J. Sellers, D. A. Randall, E. K. Schneider, J. Shukla, J. L. Kinter III, Y.-T. Hou, and E. Albertazzi, 1989: Effects of implementing the simple biosphere model in a general circulation model. *J. Atmos. Sci.,* **46,** 2757–2782.

Sellers, P. J., Y. Mintz, Y. C. Sud, and A. Dalcher, 1986: A simple biosphere model (SiB) for use within general circulation models. *J. Atmos. Sci.,* **43,** 505–531.

Sud, Y. C., J. Shukla, and Y. Mintz, 1988: Influence of land surface roughness on atmospheric circulation and rainfall: A sensitivity study with a general circulation model. *J. Appl. Meteor.,* **27,** 1036–1054.

Wang, H., and R. Fu, 2002: Cross-equatorial flow and seasonal cycle of precipitation over South America. *J. Climate,* **15,** 1591–1608.

Weaver, C. P., and R. Avissar, 2001: Atmospheric disturbances caused by human modification of the land surface. *Bull. Amer. Meteor. Soc.,* **82,** 269–281.

Webster, P. J., V. Magana, T. N. Palmer, J. Shukla, R. A. Tomas, M. Yanai, and T. Yasunari, 1998: Monsoons: Processes, predictability, and the prospects for prediction. *J. Geophys. Res.,* **103** (C7), 14 451–14 510.

Xie, P., and P. A. Arkin, 1997: Global precipitation: A 17-year monthly analysis based on gauge observations, satellite estimates, and numerical model outputs. *Bull. Amer. Meteor. Soc.,* **78,** 2539–2558.

Xue, Y., 1996: The impact of desertification in the Mongolian and the Inner Mongolian grassland on the regional climate. *J. Climate,* **9,** 2173–2189.

——, 2005: Land surface processes and monsoon. *GEWEX Newsletter*, No. 15, International GEWEX Project Office, Silver Spring, MD, 5–6.

——, P. J. Sellers, J. L. Kinter III, and J. Shukla, 1991: A simplified biosphere model for global climate studies. *J. Climate,* **4,** 345–364.

——, H. G. Bastable, P. A. Dirmeyer, and P. J. Sellers, 1996a: Sensitivity of simulated surface fluxes to changes in land surface parameterization—A study using ABRACOS data. *J. Appl. Meteor.,* **35,** 386–400.

——, M. J. Fennessy, and P. J. Sellers, 1996b: Impact of vegetation properties on U.S. summer weather prediction. *J. Geophys. Res.,* **101** (D3), 7419–7430.

——, F. J. Zeng, K. Mitchell, Z. Janjic, and E. Rogers, 2001: The impact of land surface processes on simulations of the U.S. hydrological cycle: A case study of the 1993 flood using the SSiB land surface model in the NCEP Eta Regional Model. *Mon. Wea. Rev.,* **129,** 2833–2860.

——, H.-M. Juang, W. Li, S. Prince, R. DeFries, Y. Jiao, and R. Vasic, 2004: Role of land surface processes in monsoon development: East Asia and West Africa. *J. Geophys. Res.,* **109,** D03105, doi:10.1029/2003JD003556.

Zeng, N., R. E. Dickinson, and X. Zeng, 1996: Climatic impact of Amazon deforestation—A mechanistic model study. *J. Climate,* **9,** 859–883.

Zhou, J., and K.-M. Lau, 1998: Does a monsoon climate exist over South America? *J. Climate,* **11,** 1020–1040.